International Journal of Biological Macromolecules 295 (2025) 139453

Contents lists available at ScienceDirect

International Journal of Biological Macromolecules

journal homepage: www.elsevier.com/locate/ijbiomac

Optimization of hypobaric and ultrasonic processing of persimmon rhamnogalacturonan-I to enhance drug-digestion interactions

Julio Salazar-Bermeo [a,b], Bryan Moreno-Chamba [a,b], Marta Hernández-García [a], Domingo Saura [a], Manuel Valero [a], Nuria Martí [a,*], María Concepción Martínez-Madrid [a]

[a] Instituto de Investigación, Desarrollo e Innovación en Biotecnología Sanitaria de Elche (IDiBE), Universidad Miguel Hernández, 03202 Elche, Alicante, Spain
[b] Instituto Universitario de Ingeniería de Alimentos-FoodUPV, Universitat Politècnica de València, Avenida Fausto Elio s/n, Edificio 8E, Acceso F Planta 0, 46022 Valencia, Spain

ARTICLE INFO

Keywords:
Persimmon
Bioactive polysaccharides
Dietary fiber
Vacuum instantaneous expansion
Ultrasound assisted extraction
Excipients

ABSTRACT

The biological activity of polysaccharides used for nutraceuticals/drug excipients has been a neglected area of study. This work deals with the preparation, optimization, characterization, and evaluation of persimmon (*Diospyros kaki* Thunb.) fruit by-products and the study of the resultant dietary fiber (DF) interaction with other compounds, using acetaminophen as a model. Processing conditions for persimmon by-products were optimized to enhance antioxidant activity, with hypobaric, ultrasonic, and drying conditions tested at three levels of time and pH. The optimized DF was evaluated through *in-vitro* and *ex-vivo* release and permeation studies. Optimal conditions included three cycles of vacuum instantaneous expansion coupled with ultrasound waves (USEX), 42 min of ultrasound assisted extraction (UAE), and a pH of 1.5. After treatments, the antioxidant capacity (AC) increased six-fold, and zeta potential (ζ) analysis indicated polysaccharide aggregation at the optimized pH. The optimized polysaccharides, mainly formed by rhamnogalacturonan-I, displayed nuclear factor erythroid 2-related factor 2 (Nrf2)-dependent activity. *In-vitro* drug-DF interaction studies showed higher acetaminophen release during digestion. Permeation kinetics adhered to the Korsmeyer-Peppas model in both *ex-vivo* and *in-vitro* models, suggesting complex permeation mechanisms. Results suggest that the optimized DF enhances the bioavailability and controlled release of acetaminophen, indicating its potential for use in drug delivery systems and nutraceutical applications.

1. Introduction

The upcycling of food by-products has gained increasing attention as part of a global effort to enhance sustainability and reduce waste within the food industry. Among these by-products, dietary fiber (DF) from fruits and vegetables represents a valuable resource due to its unique structural, functional, and bioactive properties [1]. DF, resistant to endogenous digestive enzymes, consists of complex polysaccharides such as hemicellulose, cellulose, homogalacturonan, arabinogalactan, and rhamnogalacturonan. These components are recognized for their roles in improving gastrointestinal health, acting as prebiotics, and serving as bioactive excipients in pharmaceutical and nutraceutical formulations [1–3]. The structural diversity of these polysaccharides enables a broad range of applications, particularly in drug delivery systems, where they can facilitate controlled release, stability enhancement, and targeted delivery of active compounds.

Persimmon (*Diospyros kaki* Thunb.) by-products, produced in large quantities during fruit production and processing, are particularly rich in bioactive DF alongside other nutritionally valuable compounds, such as polyphenols, carotenoids, and small organic acids [4,5]. The polysaccharides in persimmon by-products are distinguished for their composition, which includes monosaccharides such as fructose, rhamnose, fucose, arabinose, mannose, galactose, glucose, and uronic acids [6–8]. These polymers are further enhanced by their covalent association with bioactive compounds like trihydroxycinnamic acid (gallic acid), which imparts antioxidant properties and potential cellular modulatory effects [5,9]. While polyphenols from persimmon have been extensively studied for their antioxidant, anti-inflammatory, and

* Corresponding author.
E-mail addresses: julio.salazar@goumh.umh.es, jsalber@upv.edu.es (J. Salazar-Bermeo), bryan.morenoc@umh.es, bmorcha@upv.edu.es (B. Moreno-Chamba), m.hernandez7@goumh.umh.es (M. Hernández-García), dsaura@umh.es (D. Saura), m.valero@umh.es (M. Valero), nmarti@umh.es (N. Martí), c.martinez@umh.es (M.C. Martínez-Madrid).

https://doi.org/10.1016/j.ijbiomac.2025.139453
Received 3 September 2024; Received in revised form 24 December 2024; Accepted 1 January 2025
Available online 2 January 2025

antimicrobial activities [4–6,10–12], the technological and therapeutic applications of DF and its associated polysaccharides remain underexplored. Reports on persimmon polysaccharides emphasize their structural characteristics and functional potential, including their ability to act as gelling agents and emulsifiers in food and pharmaceutical systems [8,13]. Additionally, the structure and composition of polysaccharides may influence key biochemical pathways involved in oxidative stress, such as the nuclear factor erythroid 2-related factor 2 (Nrf2) pathway [14].

Extraction methods influence the yield, functionality, and bioactivity of polysaccharides obtained from food by-products. Traditional chemical extraction techniques often compromise the integrity of sensitive bioactive compounds, underscoring the need for sustainable and efficient alternatives. Technologies such as ultrasound-assisted extraction (UAE) and vacuum instantaneous expansion have gained traction for their ability to enhance extraction efficiency while minimizing environmental impact [15–17]. UAE relies on acoustic cavitation, where the rapid formation and collapse of bubbles generate localized energy, disrupting cell walls and releasing intracellular components [15]. This method has been widely recognized for improving the extraction efficiency of bioactive compounds, including polysaccharides, while preserving their structural integrity [17].

The integration of UAE with vacuum instantaneous expansion offers synergistic benefits for polysaccharide extraction. Vacuum expansion creates rapid pressure drops that disrupt cell walls, enhancing the accessibility of intracellular components and bioactive compounds [17]. When combined, UAE coupled to vacuum instantaneous expansion (USEX), the process further maximizes cell disintegration and the exposure of polysaccharides to the extraction medium [18]. USEX technology can improve extraction yields and maintain the functional and bioactive properties of DF, particularly when processing variables are optimized to avoid thermal or chemical degradation. For persimmon by-products, this method enables the production of polysaccharides with controlled structural and functional characteristics.

Processing variables, such as pH, temperature, and solvent composition, significantly influence the structural properties and bioactivity of DF [19]. Acidic environments are commonly employed to facilitate the release of polysaccharides and other bioactive compounds from plant matrices; these conditions may induce partial hydrolysis or structural modifications; under these conditions, the chain cleavage is specific, because of different susceptibility of the different polymer regions [20]. These conditions can also enhance functional properties like antioxidant capacity (AC), resistance to digestibility and molecular surface charge [21–23], which are variables that affect the behavior of delivery systems. Moreover, such conditions enable the simultaneous extraction of small bioactive molecules, such as phenolic compounds, adding multifunctionality to the resulting ingredients.

The ζ-potential of polysaccharides is an important parameter for assessing particle dispersion, their stability and compatibility in colloidal systems [24]. Measure of surface charge provides insights into the electrostatic interactions between polysaccharides and other components, such as drugs, bioactive compounds, or food matrices [25,26]. A controlled ζ-potential determines the compatibility of DF with other materials, facilitating its use in controlled release formulations and delivery systems. In conjunction with AC, ζ-potential serves as a key indicator of the performance and stability of polysaccharide-based matrices.

By integrating advanced extraction technologies with sustainable processing strategies, the potential of DF from persimmon by-products can be effectively achieved to develop innovative applications in food, pharmaceutical, and nutraceutical sectors. The composition, structural attributes, and bioactivity of persimmon polysaccharides highlight its potential as a versatile ingredient for enhancing the performance of bioactive delivery systems. Operating under the Generally Recognized Safe (GRAS) classification, persimmon by-products offer a range of applications, including use as nutraceutical excipients, tablet binders, disintegrants, emulsifiers, suspending agents, and gelling agents, as well as enabling colon-targeting and sustained-release formulations. The aim of this research was to evaluate the impact of USEX technology on the structural properties, antioxidant capacity, and ζ-potential of polysaccharides derived from persimmon by-products, with a focus on their potential applications in fiber-drug interactions and their development as nutraceutical excipients.

2. Materials and methods

2.1. Reagents

Ammonium acetate, formic acid, and hydrochloric acid (37 %) were obtained from PanReac (Barcelona, Spain). Acetonitrile (99.9 %), methanol (99.9 %), 1,1-diphenyl-2-picrylhydrazyl (DPPH), gallic acid, potassium bromide, glucose, arabinose, galactose, galacturonic acid, fucose, mannose, rhamnose and 1-phenyl-3-methyl-5-pyrazolone (PMP) were acquired from Merck (Madrid, Spain). Acetaminophen (APAP) was purchased from VIR S.A. (Alcorcon, Madrid, Spain). α-Amylase, pepsin, pancreatin, porcine bile extract, electrolytes ($CaCl_2$, KCl, KH_2PO_4, $NaHCO_3$, $MgCl_2$ and $(NH_4)_2CO_3$), crystal violet (CV) stain, 3-(4,5-dimethylthiazol-2-yl)-2,5-diphenyltetrazolium bromide (MTT), 2,2′-azobis(2-methylpropionamidine) dihydrochloride (AAPH), 2′,7′-dichlorodihydrofluorescein diacetate (H_2DCF-DA), 6-hydroxy-2,5,7,8-tetramethylchroman-2-carboxylic acid (Trolox) and phosphate buffered saline solution (PBS) were purchased from Sigma-Aldrich (Madrid, Spain). Dulbecco's Modified Eagle Medium (DMEM), Fetal bovine serum (SBF), penicillin, streptomycin, N-2-hydroxyethylpiperazine-N-2-ethane sulfonic acid (HEPES), 2,2′,2″,2‴-(ethane-1,2-diyldinitrilo)tetra-acetic acid (EDTA), and trypsin were purchased from Fisher Scientific (Madrid, Spain).

2.2. Plant material

Persimmon by-product batches were sourced from Mitra Sol Technologies, S.L. (Elche, Spain). The by-product, derived from 'Sharon' variety fruits, consisted of peels and pulp generated from various stages of the industrial persimmon juice production process. Samples were processed to extract carotenoids, polyphenols, and sugars, following the methodology described by Gea-Botella et al. [27]. The remaining fibers were then milled and sieved to produce uniform homogeneous samples with a diameter of 0.5 mm, which were used for this study.

2.3. By-product processing

First, the optimal parameters for the USEX system were established. Fiber samples were diluted in water at a 1:20 ratio, and pH adjustments were made to levels of 1.5, 3, and 4.5. The vacuum instantaneous expansion was conducted at a flow rate of 120 mL/min, −0.92 atm pressure, and a temperature of 75 °C. This process was repeated for up to three cycles for the same sample. Following the vacuum treatment, samples were subjected to sonication for varying residence times of 15, 30, or 60 min using a 750-Watt processor (model VCX 750, Sonics & Materials, Newtown, USA). The temperature (75 °C), amplitude (40 %), and energy (330 W) were maintained consistently. ζ-potential and antioxidant capacity (AC) served as response variables, as derived from each treatment condition. AC was quantified following each vacuum cycle and sonication period. AC was determined by the DPPH radical scavenging activity assay [28]. Results were expressed as μmol of Trolox equivalents per mg of sample (μmol TE/g sample). The absorption of the samples (515 nm) was measured with a Cytation 3 Cell Imaging Multi-Mode Reader (BioTek, Minooski, Vermont, USA). Fiber particle stability and molecular weight distribution were evaluated using a dynamic light scattering (DLS) system and ζ-potential analyzer (Brookhaven Instruments Ltd., Brookhaven, USA), where 1.5 mL of samples were mixed with 1.5 mL of distilled water (1:1) and placed in a cuvette with an

electrode inserted inside. After the USEX processing, samples were dried using either a tray drying method at 60 °C or vacuum drying with a miVac Duo concentrator (Genevac™DUC-23050-B00) at 40 °C. Following the optimization of DF processing and the selection of a drying method, the optimized DF was uniformly mixed with APAP (50 % *w*/w), dried, ground, and encapsulated in soft gels for *in vitro* interaction studies.

2.3.1. Experimental design and modeling

In this study, we employed a full factorial design (FFD) with a three-level-two-factors configuration to optimize the parameters for persimmon by-product fiber processing. We focused on the interaction between the number of vacuum cycles (X_1) with pH level (X_3), and sonication time (X_2) with pH level (X_3) to evaluate the impact on AC (Y_1) and ζ-potential (Y_2). The primary goal was to maximize AC in each step while minimizing the ζ-potential, both critical factors for ensuring the fiber ability to aggregate and protect drug components against oxidative damage, prevent strong repulsive forces, and maintain stability under gastric conditions. The experimental data was fitted into a generalized second-order polynomial model, as applied in response surface methodology (RSM) [29].

2.4. DF characterization

DF polysaccharide composition, structure, and morphology analysis was performed as previously described [7]. DF was hydrolyzed and PMP-labeled for subsequent LC-MS/MS analysis. Monosaccharide identification was performed by multiple reaction monitoring (MRM) in a LC-MS/MS-8050 Shimadzu system. Chromatographic separation was conducted using a Poroshell 120 SB-C18 2.7 μm column (4.6 × 150 mm); the injection volume was 1 μL. The mobile phase consisted of 10 mmol/L of aqueous ammonium acetate solution (solvent A) and pure acetonitrile (solvent B). The gradient was as follows: 0–45 min, 20–30 % B; 45–55 min, 30–20 % B. The column was maintained at 30 °C. Following processing, DF and APAP loaded polysaccharides were subjected to Fourier-transformed infrared (FTIR) spectroscopy analysis employing the potassium bromide (KBr) disc method. This analysis was performed using a PerkinElmer Spectrum 3 FT-IR/NIR/FIR spectrometer over a frequency range between 4000 cm^{-1} and 500 cm^{-1}. The spectra were acquired as an average of 16 scans at 4 cm^{-1} resolutions. Additionally, samples were examined using a field emission scanning electron microscope (FESEM) (Sigma 300 VP model, Carl Zeiss Microscopy GmbH, Oberkochen, Germany) at 15 kV and a magnification from 50 to 250× without coating.

2.5. In vitro digestion study

The effects of process optimization on ζ-potential were assessed through an *in vitro* digestion study. APAP, a Biopharmaceutical Classification System (BCS) class 3 drug known for its high solubility and low permeability, was selected as the model drug [30]. Drugs within this classification are particularly sensitive to the influence of excipients. For these reasons, *in vitro* studies were conducted to determine the impact of APAP and optimized DF + APAP in gastrointestinal cells viability, oxidative stress, inflammation, and permeability. *In vitro* gastrointestinal digestion was simulated using a United States Pharmacopeia (USP) Dissolution Test Apparatus II, and following the INFOGEST methodology [31] adapted for fiber matrices. Prior to digestion, simulated digestion fluids were prepared. Samples encapsulated in 600 mg soft gels included processed fraction (DF + APAP 50 %), a positive control (APAP powder from a commercial capsule 50 %), a negative control (DF), and a blank (water). The simulation process included three phases: oral (2 min at 60 rpm), gastric (2 h at 60 rpm), and intestinal (2 h at 37 °C and 60 rpm). The pH, time, and simulated digestion fluids for each phase were adjusted. After each phase, a 2 mL aliquot was extracted (and replenished) to analyze the percentage of APAP released into the chyme and chyle. The samples and digested fractions were snap-frozen and stored at −80 °C for subsequent analyses.

2.6. Interaction with epithelial cells

2.6.1. DF impact in cell culture and cytotoxicity

The impact on cell viability of digested DF and its interaction with APAP was evaluated using *in vitro* cell models. The human epithelial colorectal adenocarcinoma cell line (Caco-2, HTB-37 ATCC) which also serves as a human intestinal permeation model was employed for the assays, utilizing cells between the 30th and 40th passages. Additionally, Caco-2 cells with Nrf2 knocked down (Nrf2 KD) were used to assess the antioxidative activation pathway by the processed DF. For the generation of the Nrf2 KD cells, Caco-2 cells were co-transfected with Nrf2-specific clustered regularly interspaced short palindromic repeats (CRISPR)/Cas9 knockout (KO) plasmid and homology-directed repair (HDR) plasmid using the UltraCruz® Transfection reagent kit, following manufacturer instructions (Santa Cruz Biotechnology, Inc.) [32].

For viability assays, cells were cultured at a density of 1.5×10^4 cells/mL in 96-well plates, incubated and allowed to undergo differentiation over an 8-day period. Post differentiation, cells were incubated for 24 h with two-fold serial dilutions of fractions from the *in vitro* digested chyme (50 to 6.25 %) in DMEM. The viability (%) of untreated cells served as the normalized control. Cell viability was assessed by measuring metabolic activity through the MTT assay or adhesion capacity by CV staining, as previously documented [27,33].

2.6.2. DF role in antioxidative and anti-inflammatory intracellular activity

The impact of DF process optimization in terms of AC and its interaction with APAP was assessed through inflammation and intracellular reactive oxygen species (ROS) evaluation in Caco-2 and Nrf2 KD Caco-2 cells. Intracellular ROS levels were detected by the H_2DCF-DA probe. Cells were cultured at a density of 1.5×10^4 cells/mL into 96-well black plates using an 8-day model. These cells were then challenged with AAPH (25 μM) and treated with the digested chyme, DF alone, and DF + APAP for 5 h. Following treatment, cells were rinsed and incubated with 10 μM $DCFH_2$-DA for 40 min at 37 °C. After incubation, cells were washed three times with 1 × PBS and fluorescence was measured at 490/520 nm of excitation/emission using a microplate reader. Representative micrographs were also captured during this process. For controls, cells challenged with AAPH but untreated served as negative control, while cells treated with 25 μg/mL of Trolox served as the positive control. The fluorescence results were normalized to the negative control to assess their ROS levels. Additionally, supernatants from cells exposed to AAPH were collected to measure the levels of interleukin 6 (IL-6) and interleukin 8 (IL-8) using commercial human Diaclone enzyme-linked immunosorbent assay (ELISA) kit (Diaclone SAS, Besançon, France) providing a quantitative assessment of inflammatory response.

2.7. Permeation studies

Following digestion, the impact of the interaction between DF and APAP on permeability kinetics was examined using both *in vitro* and *ex vivo* permeation models.

2.7.1. In vitro permeation studies of DF + APAP

For the *in vitro* model, 1×10^5 of Caco-2 cells were cultured in 0.4 μm pore size transwell inserts in a 6-well plate. To form a 21-day monolayer of Caco-2 cells, growth medium (2 and 3 mL of growth medium in the apical and basolateral side, respectively) was changed every two days. For the assay, growth medium in the apical side was replaced with 2 mL of the 6.25 % of digested chyme of either APAP alone or APAP + DF. Each well in this setup functioned as the basal compartment and was filled with 3 mL of pre-warmed transport buffer Hanks balanced salt solution (HBSS) containing 25 mM HEPES (HBSS/25 mM/HEPES, pH

7.4). To monitor the permeability kinetics, a 100 μL aliquot was sampled from each basal compartment every 30 min for a total duration of 4 h. After each sampling, the volume in the basal compartment was replenished with 100 μL of fresh transport buffer [33].

2.7.2. Ex vivo intestinal permeation studies of APAP

Ex vivo analysis of intestinal permeability was conducted using Franz diffusion cells employing the intraduodenal section of porcine intestine [34–37]. The tissue samples were sourced from the animal facility in Orihuela municipal slaughterhouse (Alicante, Spain), adhering to ethical principles of reduction, refinement, and replacement. Once isolated, the tissues were meticulously excised, cleaned to avoid other compounds influence, and stored in PBS at pH 6.8. The prepared intraduodenal membranes were mounted onto the receptor chambers, connected by a 9 mm diameter cavity to its respective donor compartment. The receptor chamber was filled with PBS at pH 6.8, ensuring contact with the upper membrane surface. The system was allowed a stabilization period of 30 min before the experimental procedures commenced, reducing variability that could arise from exogenous factors. For this study, a total of 1000 μL of *in vitro* digested chyme of either APAP alone or DF + APAP was introduced into the donor compartments. The system included six Franz cells (PermeGear, Hellertown, USA), which were connected to a thermostatic bath (Selecta Digiterm-100) to maintain a temperature of 37.0 ± 0.5 °C. Throughout the experiment, continuous magnetic stirring was maintained at 300 rpm to ensure uniform distribution of the test substances. At predetermined intervals following the application of the drug, 150 μL samples were extracted from the receptor compartment for high-performance liquid chromatography (HPLC) quantification. The withdrawn volumes were immediately replaced with fresh receptor buffer to maintain the integrity and volume of the samples during the experiment.

2.7.3. APAP quantification

Permeation samples were analyzed using a HPLC Agilent series 1200 (Santa Clara, California, USA) with a reverse-phase column Poroshell 120 SB-C18 2.7 μm (4.6 × 150 mm); the ultraviolet detector was set up at 243 nm (APAP λ max.). The mobile phase comprised 0.1 % formic acid as solvent A, and acetonitrile as solvent B at a flow rate of 0.4 mL/min. The injection volume was set at 10 μL. The gradient was programmed as follows: 0–10 min, 1–20 % B; 10–15 min, 20–30 % B; 15–18 min, 30–1 % B. The column was maintained at 35 °C. Linear calibration curves for APAP were generated in the range of 0 μg/mL to 0.008 μg/mL.

2.7.4. Kinetics of intestinal permeation studies

To accurately predict and correlate the *in vitro* and *ex vivo* intestinal permeation behavior of the digested capsules, it is necessary to employ a suitable mathematical model. For these reasons, the permeation kinetic data were analyzed using various mathematical models including zero-order, first-order, Higuchi, and Korsmeyer-Peppas models [38]. The use of these models for permeation kinetics can be a valuable technique. For instance, the models can describe how a drug permeates through a barrier such as the colon or the skin over time, and the release exponent can provide insights into the permeation mechanisms.

2.8. Statistical analysis

The results were analyzed using the analysis of variance (ANOVA) and the determination of coefficients R^2 and adjusted R^2. Statistical significance for the factors and their interactions was determined through the student's *t*-test at 95 % confidence level. The levels of factors were optimized to maximize the AC and minimize the surface charge employing regression analysis and 3D surface plots of the independent variables. All experiments were conducted in triplicate to ensure reliability and reproducibility of the data. For these analyses, GraphPad Prism 8.0.2 and Statgraphics Centurion 19 software packages were utilized.

3. Results and discussion

3.1. By-product processing

The influence of pH and the frequency of vacuum instantaneous expansion cycles on the AC of treated fibers is depicted in Fig. 1A. At pH 3, the AC exhibited a 70 % enhancement from the first to the second cycle, progressing to a 90 % increase from the first to the third cycle. Conversely, at pH 4.5, there was a 61 % rise from the first to the second cycle, and a notable 112 % increase from the first to the third cycle. An inverse correlation was noted in the AC upon escalating the pH from 1.5 to 3, with reductions of 57 %, 60 %, and 22 % were observed across the first, second, and third cycles, respectively. Further elevation of pH from 3 to 4.5 resulted in decreases of 68 %, 70 %, and 65 % in the AC during the corresponding cycles. The maximal AC was consistently observed at pH 1.5 in all cases regardless of the number of cycles. Values of 0.016, 0.017, and 0.02 μmol of TE per mg of fiber sample for the first, second and third cycle were observed respectively.

In terms of ζ-potential dynamics during the initial processing step, illustrated in Fig. 1B, there was a pattern of decline in particle repulsion within DF as the number of cycles increased. Specifically, at pH levels of 1.5 and 3, the particle repulsion was inversely proportional to the cycle count, whereas at pH 4.5, this relationship was directly proportional. The lowest ζ-potential values were recorded after 3 cycles at pH 1.5 with a mean of −0.314 mV ($\sigma = 1.69$).

The effects of pH and sonication duration on the AC of treated fibers are shown in Fig. 1C. At pH 3, AC exhibited a substantial enhancement of 261 % after 30 min of sonication, progressing to 294 % by 60 min. In contrast, at pH 4.5, AC initially decreased by 37 % after 30 min, subsequently recovered, and exhibited a 31 % increase by the end of 60 min. At pH 1.5, AC decreased after 30 min and returned to initial levels after 60 min of sonication. An inverse relationship was observed between pH and AC at the beginning of the treatment, indicating a pH-dependent dynamic. Notably, the highest AC was observed at pH 1.5 after just 15 min of treatment, reaching 0.028 μmol of TE per mg of DF ($p < 0.0001$).

Regarding the ζ-potential during the second processing step, as detailed in Fig. 1D, variability was noted between −2.72 mV and +5.24 mV. There was a notable variation in repulsion forces corresponding to the sonication time; the maximum range of repulsion forces was observed at 30 min of treatment, which diminished when the sonication duration was reduced to 15 min. The lowest ranges of inter-particles surface interactions corresponded to the 15-minute treatment period, while the highest ranges were observed at 30 min of treatment and pHs of 1.5 and 3.

3.2. Effect of extraction variables

3.2.1. Vacuum instantaneous expansion

This study first aimed to elucidate the interaction between pH levels and the vacuum expansion processing cycles to enhance the AC of treated by-products through RSM-FFD. Three levels based on industrial scalability and different mathematical models were employed to delineate the effects of these parameters on the AC. It was observed that as the number of cycles increased, and pH decreased, the AC of the treated fibers was maximized. The models were formulated as equations, non-significant variables were removed and the resulted first order polynomial was expressed as Eq. (1):

$$Y_1 = 0,0147 - 0,0016 \times X_3 + 0,0045 \times X_1 \quad (1)$$

where: AC (Y_1), number of vacuum expansion cycles (X_1), and pH level (X_3).

The ANOVA indicated a significant influence of the pH level (X_3) on the AC, with a F-value of 370.29 and a *p*-value <0.0001. The number of cycles also significantly affected the AC, as evidenced by a F-value of

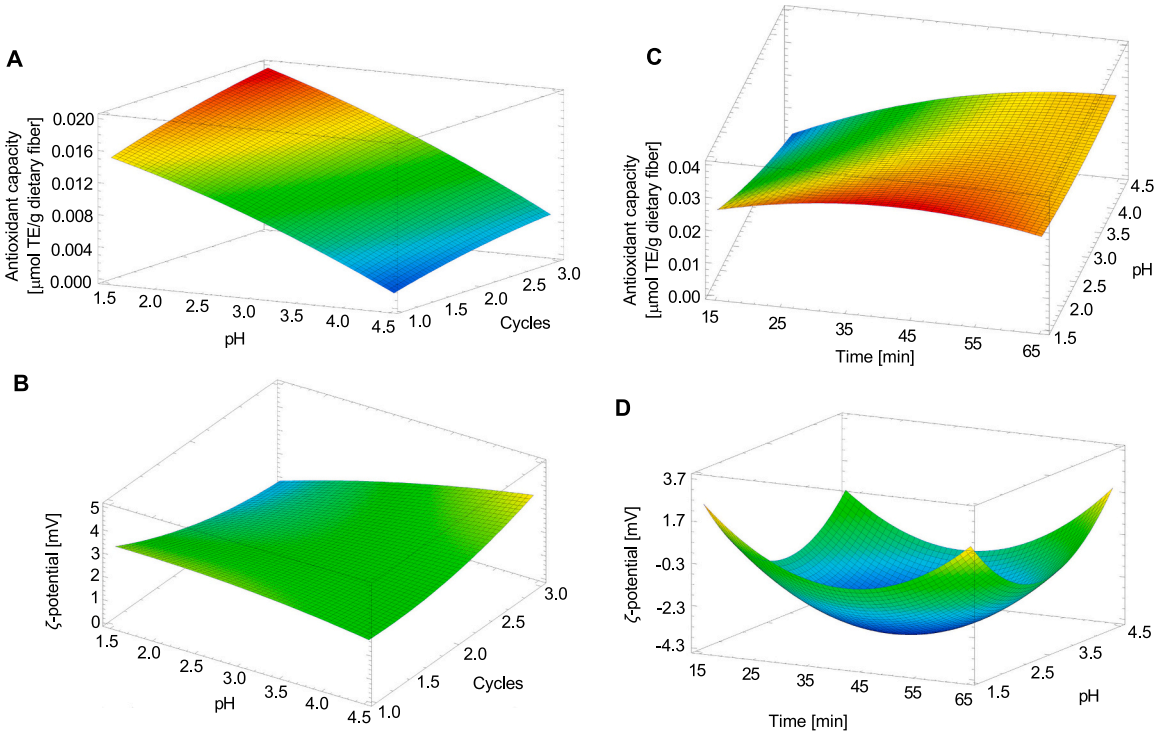

Fig. 1. Response surface plots illustrating the interaction effects of key factors on fiber processing parameters. (A) and (B) show the combined effects of vacuum instantaneous expansion cycles and pH on the antioxidant capacity (AC) and ζ-potential of the obtained fiber, respectively. (C) and (D) illustrate the interaction between sonication time and pH on the AC and ζ-potential. Antioxidant capacity is expressed as micromoles of Trolox equivalents per gram of dietary fiber (µmol TE/g), while ζ-potential is expressed in millivolts (mV). Data represent the means of three independent experiments.

32.05 and a *p*-value of 0.0024. The quadratic terms (X_1X_1 and X_3X_3) and interaction term (X_1X_3) were found to be non-significant with *p*-values >0.05. The model explained 98.7 % of the variability on the AC (R-squared = 98.7 %), with an adjusted R-squared of 97.5 %. The optimization suggested maximizing the AC at pH 1.5 and 3 cycles, leading to an optimal AC value of 0.019 µmol TE/mg fiber. During this analysis, the ANOVA showed that none of the factors or interactions exhibited a statistically significant effect on the ζ-potential at a 0.05 significance level. The highest F-value was observed in the interaction pH and cycles, with a F-value of 5.28 and a *p*-value of 0.0699, indicating a marginal trend towards significance.

Previous studies corroborate these findings, suggesting a significant effect of pH on the AC during vacuum instantaneous expansion; higher values of AC have been reported at lower pH [39] possibly due to acid hydrolysis of the fiber-bound compounds in acidic media that enhanced the release of galloylated compounds known for their AC [9,40]. These results align with findings from other studies on *Clinacanthus nutans* (Burm. f.) Lindau, where higher polyphenol content was observed by vacuum solvent-free microwave extraction (V-SFME) when the extraction was carried out under vacuum pressure compared to ambient pressure [41].

Concerning ζ-potential, increased sample aggregation at lower pHs suggested narrower ζ-potential ranges, indicative of weaker interparticle repulsions. Considering the effect of pH on AC and ζ-potential, the vacuum instantaneous expansion processing step prompted specifically higher AC and promotes initial aggregation of the fiber particles. These properties suggest potential applications of processed DFs as agglomerative agents in drugs, nutraceuticals, or food interactions, where low ζ-potential values imply minimal electrostatic repulsion and enhanced aggregation capabilities. Results were in agreement with Wang et al. [42] who processed flaxseed gum powders with different drying methods, and observed that application of vacuum led to lower ζ-potential values, in comparison to ambient pressure. The optimal results were achieved after three cycles of vacuum expansion treatment.

3.2.2. UAE

The second stage involved the application of mathematical models to describe the effects of sonication time and pH on the AC and ζ-potential through RSM-FFD. The models for ultrasound treatment demonstrated significant alignment with the experimental data, yielding R2 values 0.86 for AC and 0.93 for ζ-potential indicating minimal variation around the mean. The interaction between time (X_2) and pH level (X_3) showed a positive and significant impact on AC. Additionally, the quadratic interactions (X_2) and (X_3) were significant ($p < 0.01$) for ζ-potential. The non-significant variables were removed and the fitted first and second order polynomial Eqs. (2) and (3) were as follows:

$$Y_1 = 0,0377164 + 0,000793734 \times X_2 - 0,0175526 \times X_3 \quad (2)$$

$$Y_2 = 17,6147 + 0,00470399 \times X_2^2 + 1,34321 \times X_3^2 \quad (3)$$

where: AC (Y_1), ζ-potential (Y_2), sonication time (X_2), and pH level (X_3).

According to the ANOVA results, both (X_2) and (X_3) showed a statistically significant influence on AC, with *p*-values of 0.018 and 0.020, respectively. The model explained 86 % of the variance on AC. Optimization results suggested that the maximum AC, predicted at 0.031 µmol TE/mg fiber, could be achieved with a sonication time of 42 min and a pH of 1.5. The increase in AC following vacuum expansion processing cycles was attributed to the enhanced acid hydrolysis of DF-bound compounds through ultrasound. These findings agreed with the ones obtained by Fernandes et al. [43] who noted that lower pH levels facilitated higher extraction of antioxidant substances such as ellagic acid and anthocyanins during processing of fruit peels with UAE. The effect of sonication time was found to be pH-dependent; at lower pH levels, the highest AC observed with diminishing effects over extended sonication times. This aligns with the reports by other authors that observed increase the release of antioxidant compounds from mulberry

fruits with prolonged ultrasound exposure up to 80 min [44]. At pH 1.5, sonication time ceased to influence AC, likely due to the limits of acid hydrolysis given the composition of the matrix and the applied technology. Contrary to Fan et al. [45], who reported a decrease in the surface charge of okara fibers, the present findings suggested an initial increase in ζ-potential during the first 30 min of ultrasound treatment, followed by a decrease due to the destabilizing effects of prolonged ultrasound exposure.

The graphical representations in RSM showed AC and ζ-potential were affected by pH level, the number of vacuum expansion cycles, and sonication time. RSM plays a key role in identifying the optimum conditions for the dependent variables to achieve maximal responses [46]. The experimentally obtained values under these optimal conditions (three cycles of vacuum instantaneous expansion, 42 min of UAE, and a pH of 1.5) corroborated the predicted values. Additionally, molecular weight distribution of polysaccharides obtained under these conditions yielded an average molecular weight of 7.5×10^9 kDa which shows the structural complexity and suggests bioactivity derived from its architecture.

3.3. Drying process

Following the completion of the two by-product processing stages, the stability of the AC during the further drying was evaluated (Fig. 2). The behavior of the AC remained unaffected by the drying conditions. However, significant differences were observed between vacuum and tray methods for pH 4.5 ($p < 0.01$). At pH 1.5, where the highest AC was consistently achieved across all experiments, no effect of the different drying treatments was noted. Therefore, tray drying was selected for further use due to its practicality and greater feasibility for industrial scaling.

3.4. By-product processed fiber characterization

Optimized DF was combined with APAP, dried in trays, and subsequently characterized. Fig. 3A illustrates the morphological changes of the optimized DF before and after loading with APAP. Both DF alone and DF + APAP exhibit a homogenous reddish-brown hue, indicative of a uniform processing. DF is characterized by a densely packed collection of fragmented particles featuring highly irregular surfaces with a complex topography that includes numerous nooks and crannies. These features may significantly influence the interactions of DF within the digestive environment, food matrices, nutraceuticals or pharmaceutical

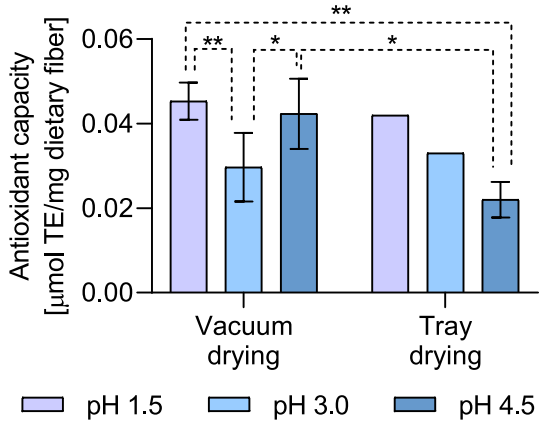

Fig. 2. Effect of vacuum and tray drying methods on the antioxidant capacity of dietary fiber (DF) from persimmon under varying pH conditions (**$p < 0.01$, *$p < 0.05$, Two-way ANOVA with Tukey's *post hoc* test). Antioxidant capacity is expressed as µmol of Trolox equivalents per mg of DF (µmol TE/mg). Results are presented as mean values ($n = 3$) ± standard deviation (SD). SD below 0.01 was not plotted.

formulations. The addition of APAP to DF slightly altered the coloration, suggesting a coating effect mediated by hydrogen bonds, hydrophobic interactions, and ion interactions influenced by the pH environment [47]. APAP + DF images show a less defined and more integrated structure compared to the granular nature of the DF alone. At a higher magnification of 40 µm, the particles exhibit a layering effect, indicative of APAP adhesion, which results in a smoother and more consolidated surface architecture. This amalgamation creates a matrix distinct from the standalone DF, with APAP filling the interstitial spaces, reducing the surface roughness, and forming a more homogenized structural composite. The resultant morphology suggests a potential modification in the functional properties of DF, such as solubility, binding capacity, and possibly the rate of release or permeation in physiological environments. Both macroscopic and microscopic evaluation provide a comprehensive understanding of the structural dynamics at play. These characterizations are useful for predicting the interactive behaviors of DF when combined with other compounds such as foods, nutraceuticals, and drugs, thereby providing information their optimized application in various formulations.

The FTIR spectra of persimmon DF revealed complex composition of functional groups from polysaccharides and phenolic compounds, as depicted in Fig. 3B. For instance, a strong and broad peak at 3391.79 cm^{-1} was noted, characteristic of the O—H stretching vibrations typically found in cellulose, hemicellulose, and tannic acid, components prevalent in DF [48,49]. Peaks at 2926–2925 cm^{-1} were observed for methylene groups, confirming the presence of cellulose and other saccharides structures [48,50]. Sharp absorption between 1615 and 1610 cm^{-1} for free carboxylic groups in gallotannins was also noted [51,52], relevant for their role in the AC of DFs. A weaker peak at 1531.18 cm^{-1}, corresponding to phenolic type proanthocyanidins [53,54],suggests the presence of complex phenolic compounds previously reported by Moreno-Chamba et al. [9] and Salazar-Bermeo et al. [7]. Additionally, O—H groups associated with covalently bonded phenolics were identified at 1233–1227 cm^{-1} [53,55,56], reflecting the conjugation of polyphenols to the persimmon polymeric matrix in DF. Methylene groups, indicative of the structural integrity of rhamnose and cellulose, were confirmed at 1371–1370 cm^{-1} [51,52]. Furthermore, glycosidic bonds from the structural framework of DF were detected at 1150.12 cm^{-1} and 1108–1105 cm^{-1}. These bonds link galacturonic acid, mannose-containing hemicellulose, cellulose, and other polysaccharides [13,48,51,52,56] concerning the carbohydrate structure of this matrix. Additional peaks related to the glycosidic links of arabinose-based glucans and arabinoxylans were evident at 1022.74 cm^{-1} [13,51–53,57]. Peaks below 900 cm^{-1}, indicative of C-6 units and skeletal bending of galactose [48,58] are typical of the monosaccharide components of pectin and hemicelluloses.

In the DF + APAP interaction, distinct peaks at 3161.89 cm^{-1} were attributed to phenolic structures, while minor peaks at 3109.29 cm^{-1} and 3034.65 cm^{-1} indicated C—H (methyl groups) and aromatic C—H bonds, respectively [56,59,60], suggesting subtle chemical interactions. Sharp amide peaks at 3326.53 cm^{-1} were noted from the APAP loading, with further evidence of amide and C—O functional groups at 2976.54 cm^{-1}, 2926–2925 cm^{-1}, and 1610.85 cm^{-1}, respectively [59–61]. Aromatic combination bands and amide groups were observed between 2035 and 1827 cm^{-1} and at 1565 cm^{-1}, complemented by pronounced methyl peaks at 1506.86 cm^{-1}, and peaks aligned with C-OH bending, CH rocking, and C—C stretching at 1327.69 cm^{-1} [60]. Strong peaks at 1259 cm^{-1} and 1243.41 cm^{-1} were indicative of the aryl group and C═O in esters and epoxides, with additional peaks at 1233–1227 cm^{-1} related to hydroxybenzene structures. Physiosorbed carbon dioxide and phenyl deformations in APAP were identified by peaks at 686.42 cm^{-1} and out-of-plane deformations of the phenyl ring at 518.91 cm^{-1} [59,62].

The primary monosaccharides identified in the DF structure from persimmon processed insoluble DF included glucose (D-Glu), arabinose (Ara), galactose (Gal), galacturonic acid (GalA), fucose (L-Fuc),

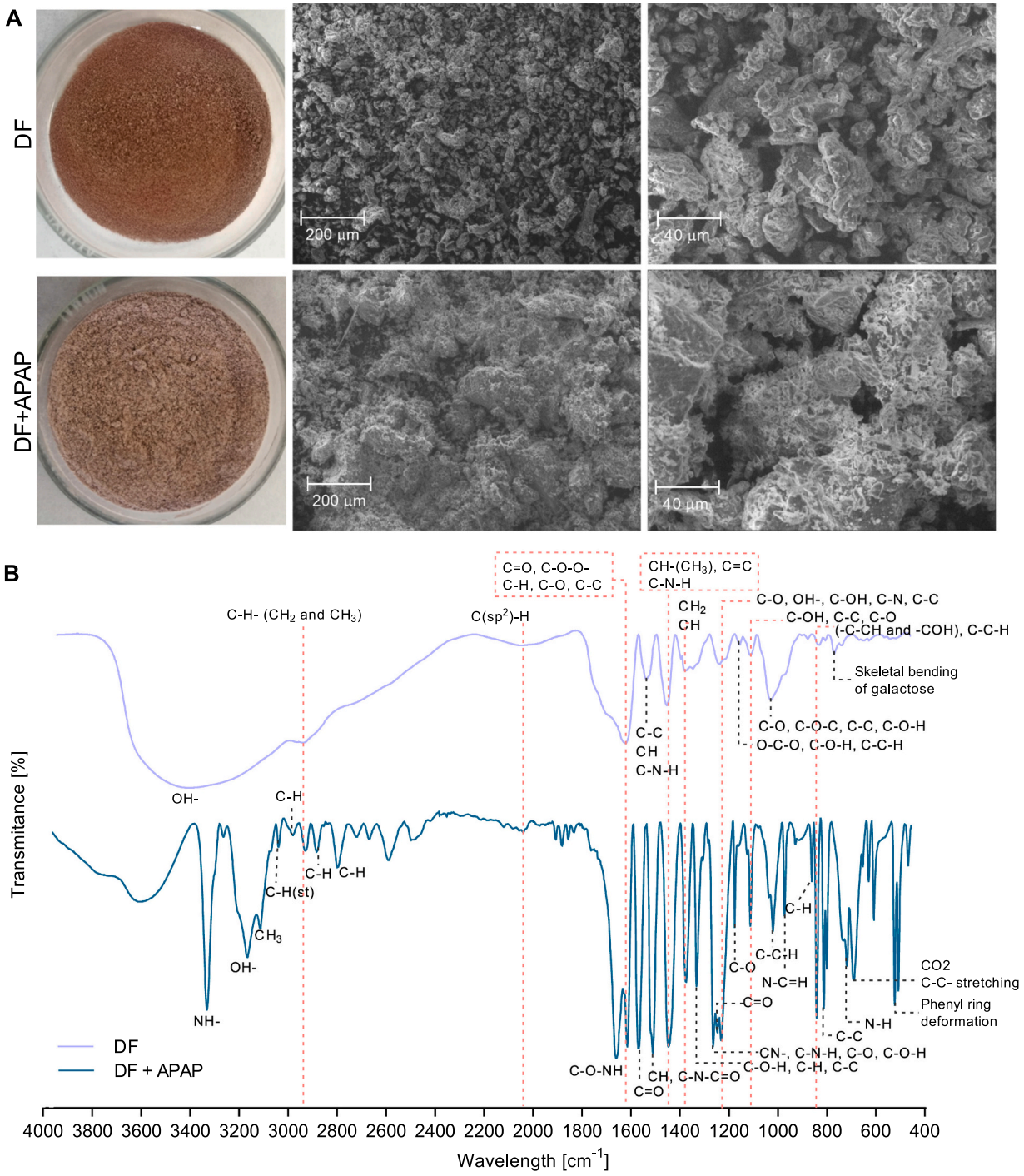

Fig. 3. (A) Field emission scanning electronic microscope micrographs of persimmon dietary fiber (DF) and DF loaded with acetaminophen (DF + APAP). (B) Fourier-transform infrared (FTIR) spectra of persimmon DF and DF + APAP. Common functional groups (peaks) in the samples are shown in red segmented lines.

mannose (D-Man), and rhamnose (D-Rha), as shown in Fig. 4A. Consistent with previous findings, Ara, D-Glu, and D-Gal emerged as the most abundant monosaccharides within the persimmon insoluble DF. Molar ratios presented in Fig. 4B suggest a prominent rhamnogalacturonan (RG-I) domain with limited branching, as indicated by the ratio of (Gal + Ara) to Rha. The relatively low value of GalA/(Ara + Gal + Rha) implies a structure with limited linear chains, while the ratio of Gal/Rha points to RG-I regions featuring extended galactan side chains. Recent studies have reported a structure of rhamnogalacturonan-I (RG-I) with a higher degree of branching, or the predomination of a homogalacturonan-I domain in persimmon by-products [7,48]. These observations were made under different processing conditions. Consequently, these alterations influence the composition and functional properties of the fibers, affecting their potential applications. A comprehensive understanding of these relationships is crucial for optimizing the utilization of persimmon DF in various industries.

3.5. *In vitro gastrointestinal digestion*

In the gastric phase, the results diverged from common expectation (Fig. 5); DF did not slow down the release of APAP but appeared to have promoted it when compared to the commercially available APAP. This

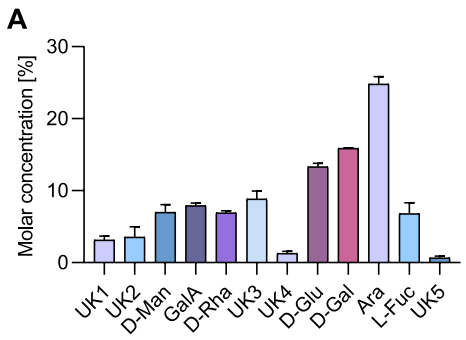

B

Monosaccharide molar ratio						
GalA / Rha	Gal+Ara / Rha	Rha / GalA	Gal / Ara+Gal+Rha	RG-I	HG	HG / RG-1
1.15	5.88	0.88	0.17	54.51	8.94	0.17

Fig. 4. (A) Molar concentration of monosaccharides in persimmon insoluble dietary fiber (DF) after optimized vacuum expansion and sonication processes. Data are presented as mean (n = 3) ± standard deviation. Abbreviations: D-Man, mannose; GalA, galacturonic acid; D-Rha, rhamnose; D-Glu, glucose; D-Gal, galactose; Ara, arabinose; L-Fuc, fucose; UK, unknown compounds. (B) Calculated molar ratio of monosaccharides found in persimmon insoluble DF. Abbreviations: RG-I, rhamnogalacturonan-I; HG, homogalacturonan. Molar ratio values are dimensionless.

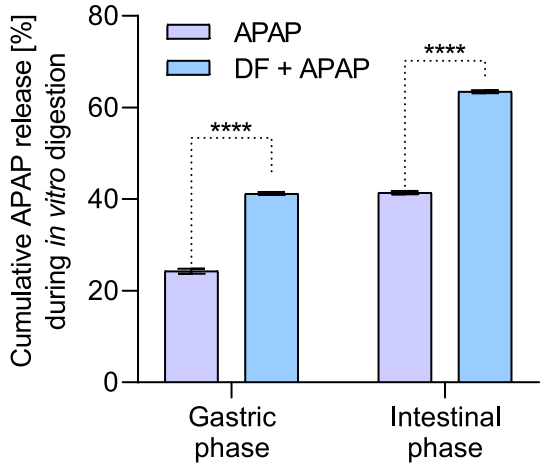

Fig. 5. Percentage of the total initial amount of acetaminophen (APAP) alone or with dietary fiber (DF + APAP) that was accumulated during gastric and intestinal phases of the *in vitro* digestion process. (****$p < 0.0001$, One-way ANOVA with Student's *t*-test). Results are shown as mean (n = 3) ± standard deviation (SD).

observation suggests that the technological adjustments made in optimizing DF, such as pH of fiber, may influence the release kinetics of its associated molecule, in this scenario, APAP potentially modulating its release in the stomach. During the intestinal phase, the bioavailability of APAP increased significantly for both conditions. In particular, the increase in bioavailability was more pronounced with the APAP + DF combination, indicating a synergistic effect of DF on the drug release to the intestinal region. Specifically, 25 % and 44 % of APAP were released from the matrix after the corresponding gastric digestion phases of APAP alone and DF + APAP respectively, while 66 % and 86 % were released after the respective intestinal phases for APAP and DF + APAP.

The presence of DF appears to influence the release profile of APAP, which could have significant implications for the drug absorption and overall bioavailability. A delayed gastric release may result in a slower onset of action, while an enhanced intestinal release might lead to an increased or more sustained absorption in the latter part of the digestive tract. The modulation of bioavailability by DF could potentially lead to variations in the interacting molecule bioactive potential and side effects. For instance, a slower release in the gastric phase may reduce gastrointestinal side effects, while the enhanced release in the intestinal phase, observed in Fig. 5, could enhance efficacy or, conversely, heighten the risk of systemic side effects if the absorption occurs too rapidly. In this study, the insoluble DF of persimmon by-product was utilized. Similar experiments have also been conducted with cellulose, pectin or chitosan derived from various sources, to create matrices that act as controlled release carriers. These methods have involved different active ingredients including surfactants, lipids, polyethylene glycol (PEG), and poly(D,L-lactide-co-glycolide) acid (PLGA), which typically require additional processing steps [63–65].

Optimized DF matrix obtaining process resulted in a structure that was both more porous and reactive, which facilitated improved adsorption and release of APAP. These optimized matrix characteristics contributed to a uniform coating of APAP, which in turn influenced its release profile, leading to a consistent and sustained release in the gastrointestinal environment. Within the process, ultrasonic treatment may have influenced the DF matrix by enhancing surface properties and increasing AC, which may have implications for the binding and release characteristics of APAP within the DF matrix. Moreover, the increase in AC, which was pH-dependent, indicates that the matrix reactivity and solubility may be optimized for acidic environments, such as the stomach. This could facilitate the initial release of APAP and potentially influence its subsequent release rate in the intestine. The presence of specific functional groups in the DF matrix, such as O—H associated with cellulose and tannic acid, methylene groups, and free carboxylic groups in gallotannins, may be playing an important role in the binding and releasing DF capabilities. The consolidated surface of the matrix seemed to promote a gradual and sustained release, particularly in the intestinal phase, where an increase in bioavailability was noted.

3.6. *Effect of APAP and DF + APAP on Caco-2 cells*

The viability results on Caco-2 (Fig. 6A and B) and Nrf2 KD Caco-2 (Fig. 6B) cells showed a significant reduction on cell survival for digested APAP and DF + APAP at concentrations above 0.5 mg/mL of APAP. Notably, DF + APAP exhibited the highest cell survival rates across both cell models, even at higher concentrations, demonstrating fewer adverse effects on cell viability compared to APAP alone. In the case of CV staining, higher cell survival rates were observed for both APAP and DF + APAP in the two cell models with the most favorable viability observed at 0.5 mg/mL. These findings suggest that the digested fractions may exert protective effects on cell metabolism. However, this protective effect was diminished in the Nrf2 KD Caco-2 cells, highlighting the role of Nrf2 in mitigating the cytotoxic effects of APAP. Consequently, the lowest concentrations tested (0.5 mg/mL) was used for the following *in vitro* assays.

Intracellular ROS assessment following AAPH-induced oxidative damage in Caco-2 cells (Fig. 7A) demonstrated that DF reduced ROS levels, achieving a similar to the action of Trolox (the reference antioxidant) and surpassing the antioxidant potential of APAP alone. In contrast, in the absence of DF, intracellular ROS levels remained higher, indicating that DF contributes additional antioxidant activity. This effect however, was not observed in Nrf2 KD Caco-2 cells where ROS levels remained elevated regardless of the presence of APAP or DF + APAP (Fig. 7B). This discrepancy highlights the pivotal role of the Nrf2 pathway in mediating the antioxidant effects of DF. Previous studies have shown that polysaccharides with higher contents of GalA or GlcA, as well as Ara, Gal, and Rha, can elevate mRNA and protein expression of Nrf2, promoting its activation. Additionally, shorter side chains in polysaccharides are more effective in enhancing Nrf2 activity, a potential mechanism for the observed reduction in ROS levels [14]. The cellular AC appears to be directly linked to the functional groups within DF matrix identified by the FTIR spectroscopy, including hydroxyl

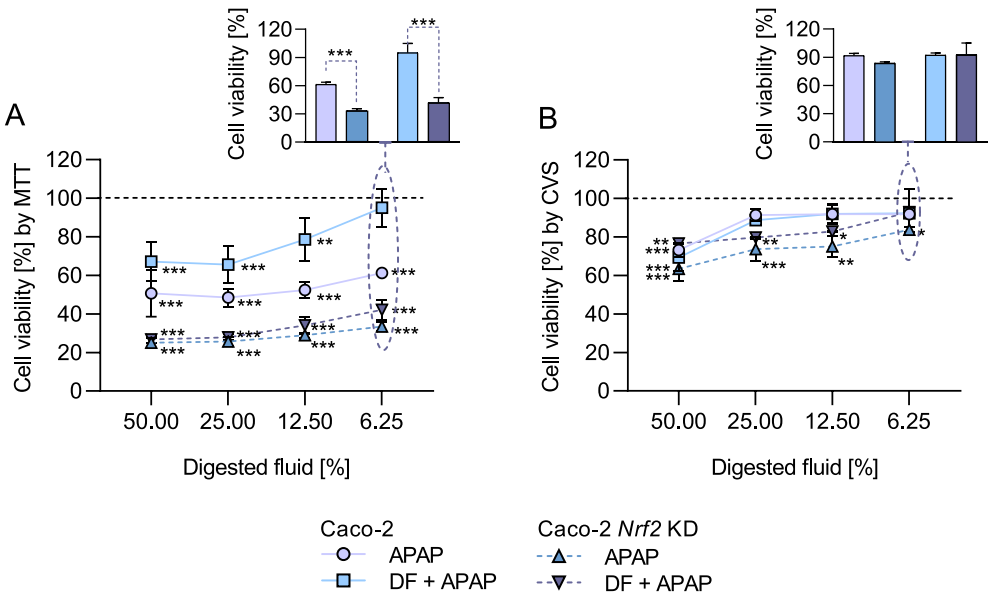

Fig. 6. Viability of human adenocarcinoma colon cells (Caco-2) and Nrf2 knockdown Caco-2 (Nrf2 KD Caco-2) cells after treatment with digested acetaminophen (APAP) or persimmon dietary fiber loaded with APAP (DF + APAP) at varying doses. Cell viability was assessed using the (A) MTT assay and (B) crystal violet staining. Comparisons were made to untreated cells (***$p < 0.001$, **$p < 0.01$, *$p < 0.05$; One-way ANOVA with Dunnett's *post hoc* test). The final growth of Caco-2 and Nrf2 KD Caco-2 cells at the highest dose of both APAP and DF + APAP was also analyzed (***$p < 0.001$; One-way ANOVA with Student's *t*-test). Results are shown as mean (n = 3) ± standard deviation.

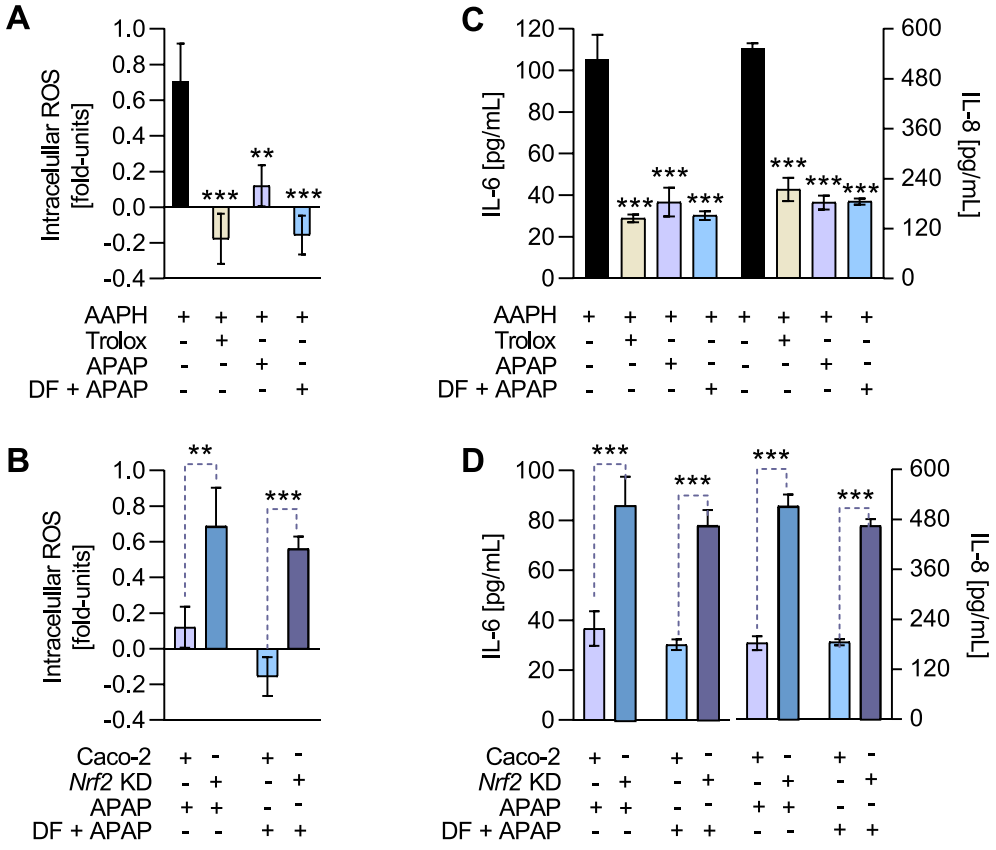

Fig. 7. Modulation of (A) intracellular reactive oxygen species (ROS) and (C) pro-inflammatory interleukin 6 (IL-6) and 8 (IL-8) in stressed human adenocarcinoma colon (Caco-2) cells treated with digested acetaminophen (APAP) and persimmon dietary fiber loaded with APAP (DF + APAP). Trolox was used as positive control. Results were compared to AAPH challenged cells (negative control) (***$p < 0.001$, **$p < 0.01$; One-way ANOVA with Dunnett's *post hoc* test). (B) Comparison of intracellular ROS and (D) IL-6 and IL-8 levels between Caco-2 and Nrf2 knockdown Caco-2 (Nrf2 KD Caco-2) cells treated by both APAP or DF + APAP (***$p < 0.001$, **$p < 0.01$; One-way ANOVA with Student's *t*-test). Results are shown as mean (n = 3) ± standard deviation.

groups (from glucose and polyphenol residues), free carboxylic groups, and shorter polymeric units released during gastrointestinal digestion. These groups may interact with cellular pathways, activating the Nrf2 as part of a xenobiotic response [66].

Regarding inflammation markers, given that APAP is an anti-inflammatory drug, all AAPH challenged Caco-2 cells responded similarly in the presence of Trolox, APAP or DF + APAP with significant reductions in IL-6 and IL8 levels (Fig. 7C), achieving up to a 60 % reduction in proinflammatory markers. In contrast, this anti-inflammatory action was not observed in Nrf2 KD Caco-2 cells under any treatment conditions (Fig. 7D). These findings are consistent with the notion that DF may enhance the anti-inflammatory effects of APAP through Nrf2-mediated pathways (Fig. 8), where Trolox treated cells displayed minimal fluorescence from the $DCFH_2$-DA probe, whereas APAP-treatment resulted in elevated ROS production in both Caco-2 and Nrf2 KD Caco-2 cell lines. The addition of DF mitigated ROS expression in wild-type cells, although levels remained elevated compared to Trolox treatment. The results suggest that the antioxidant effects of DF are partly mediated by the Nrf2 pathway and are influenced by its structural features, such as the functional groups and shorter polysaccharide chains released during digestion.

3.7. Permeability in the small intestine

In vitro and *ex vivo* intraduodenal permeation assays were employed to evaluate the effects of previously digested and released APAP (Fig. 9). The results were compared to corresponding control samples without DF. Intraduodenal analysis of samples taken measured at multiple time-points revealed that DF + APAP *ex vivo* and *in vitro* permeation kinetics behaved similarly. For the *ex vivo* model in presence of DF (Fig. 9A), APAP permeated 29 % of the total released APAP after *in vitro* digestion, at the latest time-point checked (4 h). Similarly, in the *in vitro* model (Fig. 9B), 23 % of the total released APAP in presence of DF permeated after 4 h. In contrast, APAP alone exhibited a marginally slower permeation rate; 20 % of the drug permeated after 4 h in the *ex vivo* model, and 21 % permeated in the *in vitro* model. Given the comparable performance of both models, the *ex vivo* model is recommended due to its speed, ease and reproducibility making it a more efficient choice for testing drug permeation kinetics.

To determine whether the presence of DF influenced the permeation rates following *in vitro* digestion, permeation dynamics were studied both *in vitro* and *ex vivo*. The release profiles of APAP and DF + APAP displayed similar curves, indicating an increase in the amount of APAP liberated without altering the overall dynamic profile in both models. Efforts to fit the observed data to four classical kinetic release models are summarized in Fig. 9C. According to the analysis, all samples followed the Korsmeyer-Peppas model; notably, for the *ex vivo* model, the permeation exponent (n) or the diffusion exponent found to exceed 1, suggesting that the drug permeation from the system is linked to complex processes [67] that need to be studied. This observation implies that the permeation may have been ruled by barrier swelling, erosion, or drug-barrier interactions and by the macromolecular relaxation of the tight junctions within the tissue network. Particularly, this event was higher for APAP alone, a lower n may imply lower sensitivity to environmental factors and might be more suitable for conditions needing a more sustained release during gastrointestinal digestion. Conversely, in the *in vitro* model, Fickian diffusion was observed, likely due to the absence of the macromolecular relaxation events in the Caco-2 cell monolayer.

The unique properties of rhamnogalacturonan-I from persimmon by-products position it distinctly among other polysaccharides used in drug delivery systems. Unlike soluble fibers obtained from citrus fruits such as homogalacturonans or arabinogalactans, which enhance drug release through gelation or molecular complexation [68], persimmon's rhamnogalacturonan-I surface charge behavior enables modulation of drug release in both gastric and intestinal phases. Specifically, its ability to promote gastric phase release and synergistically enhance intestinal bioavailability is distinct from cellulose, which typically delays release, or chitosan, which requires blending with excipients for similar effects [69]. These properties suggest that persimmon DF acts through a combination of surface interactions and matrix modulation to protect and enhance the release of active compounds.

4. Conclusions

The extraction process optimization, including vacuum instantaneous expansion, UAE, and detailed characterization, significantly enhanced the obtained DF matrix properties inclusive of AC by optimizing pH levels, the number of vacuum expansion cycles, and the sonication time, which provides a more porous and reactive surface. The enhanced AC, particularly with three cycles of vacuum expansion, 42 min of UAE, and a pH of 1.5, created a matrix that facilitated better

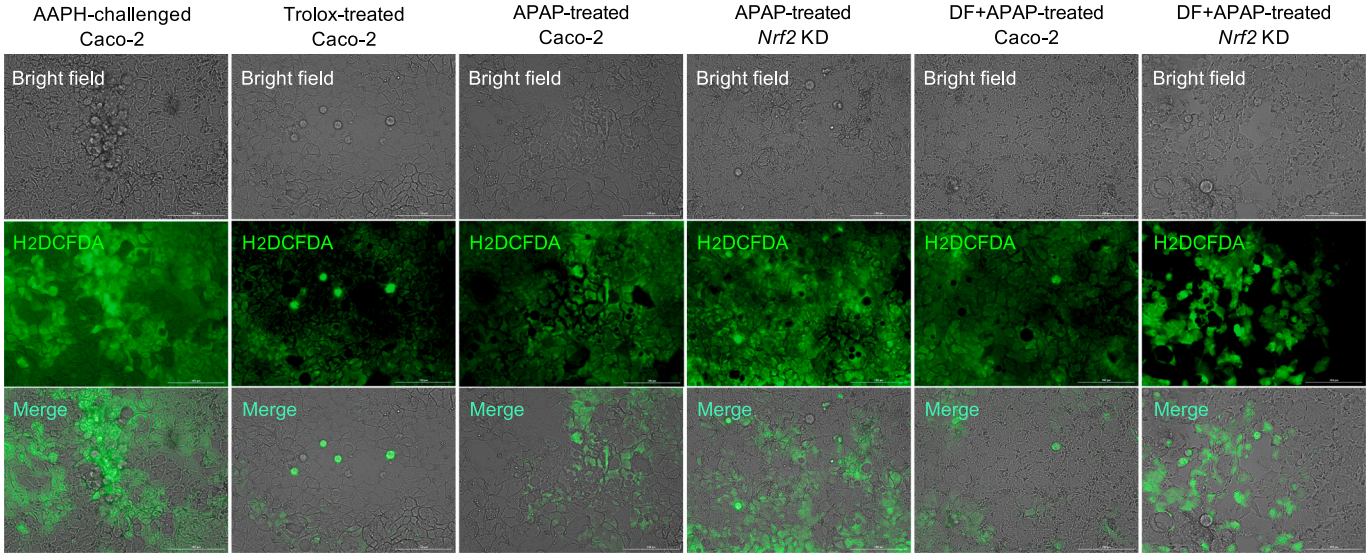

Fig. 8. Representative micrographs of the intracellular reactive oxygen species induced by AAPH (negative control) in human adenocarcinoma colon cells (Caco-2) and Nrf2 knockdown Caco-2 (Nrf2 KD Caco-2) cells labeled with H_2DCFDA. Images of cells treated with Trolox (positive control), acetaminophen (APAP), and persimmon dietary fiber loaded with APAP (DF + APAP) are also shown.

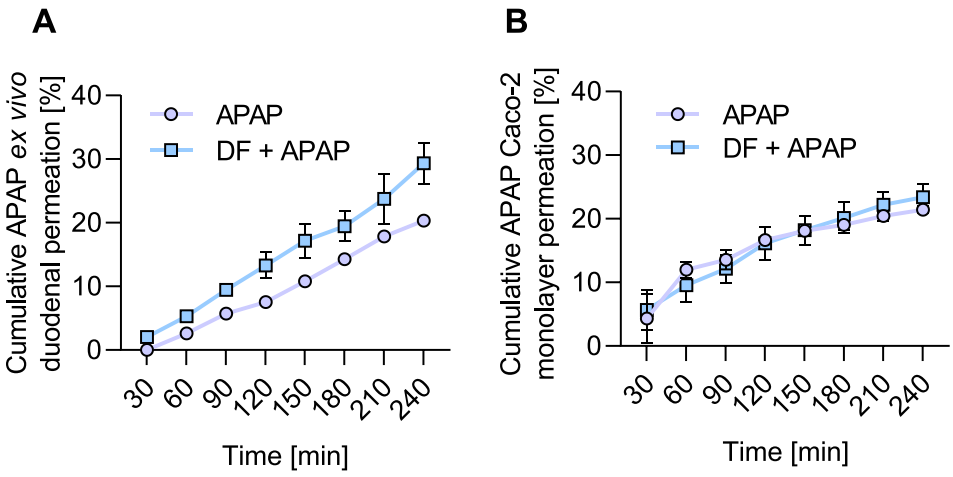

C

Sample	Zero order		First order		Higuchi		Korsmeyer-Peppas		
	K_0	R^2	K_1	R^2	K_H	R^2	K	n	R^2
Ex vivo permeation									
APAP	0.08	0.94	0.00	0.92	1.00	0.65	**0.01**	**1.46**	**0.99**
DF+APAP	0.10	0.85	0.01	0.82	1.21	0.58	**0.04**	**1.22**	**0.99**
In vitro Caco-2 permeation									
APAP	0.14	0.87	0.00	0.93	1.79	0.95	**0.72**	**0.68**	**0.99**
DF+APAP	0.11	0.86	0.00	0.91	1.45	0.95	**0.53**	**0.70**	**0.99**

Fig. 9. (A) *Ex vivo* intraduodenal and (B) *in vitro* human adenocarcinoma colon cell (Caco-2) monolayer permeation of digested acetaminophen (APAP) and dietary fiber loaded with APAP (DF + APAP). (C) Kinetic parameters from *ex vivo* and *in vitro* permeation models for the drug-fiber interaction. Optimal parameter fits are highlighted in bold. Results are presented as mean (n = 3) ± standard deviation.

interaction with APAP. The uniform and integrated structure of DF + APAP indicated effective coating and binding of APAP, contributing to modified release, permeation, and overall bioavailability properties. DF + APAP modulated the oxidative stress response through the intestinal barrier by maintaining cell viability and function. These results suggest persimmon byproducts processed fiber as a suitable material for its application as a functional excipient within the food, nutraceutical, and pharmaceutical areas.

CRediT authorship contribution statement

Julio Salazar-Bermeo: Writing – original draft, Visualization, Methodology, Investigation, Formal analysis, Data curation, Conceptualization. **Bryan Moreno-Chamba:** Writing – original draft, Visualization, Methodology, Investigation, Formal analysis, Data curation. **Marta Hernández-García:** Writing – original draft, Visualization, Methodology, Investigation, Formal analysis, Data curation. **Domingo Saura:** Supervision, Project administration, Funding acquisition, Conceptualization. **Manuel Valero:** Writing – review & editing, Supervision, Conceptualization. **Nuria Martí:** Supervision, Project administration, Funding acquisition, Conceptualization. **María Concepción Martínez-Madrid:** Validation, Supervision, Conceptualization.

Funding

This study was supported by Ministerio de Ciencia, Innovación y Universidades through the funded project 'Simbiosis industrial en el aprovechamiento integral del caqui (*Diospyros kaki*); Ejemplo de bioeconomía' (CTM2017-88978-R), and by the predoctoral fellowship of J. S.-B. from Miguel Hernández University ("Ayudas a la contratación de personal investigador en formación 2022").

Declaration of competing interest

The authors declare that they have no known competing financial interests or personal relationships that could have appeared to influence the work reported in this paper.

Data availability

Data will be made available on request.

References

[1] F.T. Macagnan, L.P. da Silva, L.H. Hecktheuer, Dietary fibre: the scientific search for an ideal definition and methodology of analysis, and its physiological importance as a carrier of bioactive compounds, Food Res. Int. 85 (2016) 144–154, https://doi.org/10.1016/j.foodres.2016.04.032.

[2] B.R. Shah, B. Li, H. Al Sabbah, W. Xu, J. Mráz, Effects of prebiotic dietary fibers and probiotics on human health: with special focus on recent advancement in their encapsulated formulations, Trends Food Sci. Technol. 102 (2020) 178–192, https://doi.org/10.1016/j.tifs.2020.06.010.

[3] M.N. Motiwala, M.N. Dumore, V.V. Rokde, M.M. Bodhe, R.A. Gupta, N.G. Dumore, K.R. Danao, Characterization and antioxidant potential of *Coccinia indica* fruit mucilage: evaluation of its binding properties, Bioact. Carbohydr. Diet. Fibre 6 (2015) 69–74, https://doi.org/10.1016/j.bcdf.2015.09.001.

[4] S. Gea-Botella, B. Moreno-Chamba, L. de la Casa, J. Salazar-Bermeo, N. Martí, M. C. Martínez-Madrid, M. Valero, D. Saura, Carotenoids from persimmon (*Diospyros kaki* Thunb.) byproducts exert photoprotective, antioxidative and microbial anti-adhesive effects on HaCaT, Pharmaceutics 13 (2021) 1898, https://doi.org/10.3390/pharmaceutics13111898.

[5] B. Moreno-Chamba, J. Salazar-Bermeo, P. Navarro-Simarro, M. Narváez-Asensio, M.C. Martínez-Madrid, D. Saura, N. Martí, M. Valero, Autoinducers modulation as a potential anti-virulence target of bacteria by phenolic compounds, Int. J. Antimicrob. Agents 62 (2023) 106937, https://doi.org/10.1016/j.ijantimicag.2023.106937.

[6] L. López-Bermudo, B. Moreno-Chamba, J. Salazar-Bermeo, N.J. Hayward, A. Morris, G.J. Duncan, W.R. Russell, A. Cárdenas, Á. Ortega, B. Escudero-López, G. Berná, N. Martí Bruña, S.H. Duncan, M. Neacsu, F. Martin, Persimmon fiber-rich ingredients promote anti-inflammatory responses and the growth of beneficial anti-

inflammatory Firmicutes species from the human colon, Nutrients 16 (2024) 2518, https://doi.org/10.3390/nu16152518.
[7] J. Salazar-Bermeo, B. Moreno-Chamba, R. Heredia-Hortigüela, V. Lizama, M. C. Martínez-Madrid, D. Saura, M. Valero, M. Neacsu, N. Martí, Green technologies for persimmon by-products revalorisation as sustainable sources of dietary fibre and antioxidants for functional beverages development, Antioxidants 12 (2023) 1085, https://doi.org/10.3390/antiox12051085.
[8] S. Gorinstein, Z. Zachwieja, M. Folta, H. Barton, J. Piotrowicz, M. Zemser, M. Weisz, S. Trackhtenberg, O. Màrtin-Belloso, Comparative contents of dietary fiber, total phenolics, and minerals in persimmons and apples, J. Agric. Food Chem. 49 (2) (2001) 952–957, https://doi.org/10.1021/jf000947k.
[9] B. Moreno-Chamba, J. Salazar-Bermeo, M.C. Martínez-Madrid, V. Lizama, F. Martín-Bermudo, G. Berná, M. Neacsu, D. Saura, N. Martí, M. Valero, Bound galloylated compounds in persimmon upcycled dietary fiber modulate microbial strains associated to human health after *in vitro* digestion, LWT - Food Sci. Technol. 156 (2022) 113011, https://doi.org/10.1016/j.lwt.2021.113011.
[10] M.S. Butt, M.T. Sultan, M. Aziz, A. Naz, W. Ahmed, N. Kumar, M. Imran, Persimmon (*Diospyros kaki*) fruit: hidden phytochemicals and health claims, EXCLI J. 14Doc542 ISSN (2015) 1611–2156, https://doi.org/10.17179/EXCLI2015-159.
[11] Y. Matsumura, T. Ito, H. Yano, E. Kita, K. Mikasa, M. Okada, A. Furutani, Y. Murono, M. Shibata, Y. Nishii, S. Kayano, Antioxidant potential in non-extractable fractions of dried persimmon (*Diospyros kaki* Thunb.), Food Chem. 202 (2016) 99–103, https://doi.org/10.1016/j.foodchem.2016.01.112.
[12] R. Direito, J. Rocha, A.-T. Serra, A. Fernandes, M. Freitas, E. Fernandes, R. Pinto, R. Bronze, B. Sepodes, M.-E. Figueira, Anti-inflammatory effects of persimmon (*Diospyros kaki* L.) in experimental rodent rheumatoid arthritis, J. Diet. Suppl. 17 (2020) 663–683, https://doi.org/10.1080/19390211.2019.1645256.
[13] Y. Jiang, Y. Xu, F. Li, D. Li, Q. Huang, Pectin extracted from persimmon peel: a physicochemical characterization and emulsifying properties evaluation, Food Hydrocoll. 101 (2020) 105561, https://doi.org/10.1016/j.foodhyd.2019.105561.
[14] J.-H. Luo, J. Li, Z.-C. Shen, X.-F. Lin, A.-Q. Chen, Y.-F. Wang, E.-S. Gong, D. Liu, Q. Zou, X.-Y. Wang, Advances in health-promoting effects of natural polysaccharides: regulation on Nrf2 antioxidant pathway, Front. Nutr. 10 (2023), https://doi.org/10.3389/fnut.2023.1102146.
[15] C. Wen, J. Zhang, H. Zhang, C.S. Dzah, M. Zandile, Y. Duan, H. Ma, X. Luo, Advances in ultrasound assisted extraction of bioactive compounds from cash crops - a review, Ultrason. Sonochem. 48 (2018) 538–549, https://doi.org/10.1016/j.ultsonch.2018.07.018.
[16] F. Chemat, M.K. Zill-e-Huma, Khan, applications of ultrasound in food technology: processing, preservation and extraction, Ultrason. Sonochem. 18 (2011) 813–835, https://doi.org/10.1016/j.ultsonch.2010.11.023.
[17] S. Roohinejad, M. Koubaa, F.J. Barba, R. Greiner, V. Orlien, N.I. Lebovka, Negative pressure cavitation extraction: a novel method for extraction of food bioactive compounds from plant materials, Trends Food Sci. Technol. 52 (2016) 98–108, https://doi.org/10.1016/j.tifs.2016.04.005.
[18] D. Saura-López, N. Martí-Bruñá, M. Valero-Roche, E. Bernal-Belda, S. Vegara-Gómez, M.de los R. Berenguer-Martínez, V. Micol-Molina, Apparatus for instantaneous expansion with vacuum and ultrasound waves, EP2915437A1 11 (2015), https://worldwide.espacenet.com/patent/search/family/050067451/publication/US2015258225A1?q=domingo%20saura%20Miguel%20hern%C3%A1ndez. (Accessed 12 December 2020).
[19] F. Guillon, M. Champ, Structural and physical properties of dietary fibres, and consequences of processing on human physiology, Food Res. Int. 33 (2000) 233–245, https://doi.org/10.1016/S0963-9969(00)00038-7.
[20] M. Ulbrich, J.M. Daler, E. Flöter, Acid hydrolysis of corn starch genotypes. I. Impact on morphological and molecular properties, Carbohydr. Polym. 219 (2019) 172–180, https://doi.org/10.1016/j.carbpol.2019.05.010.
[21] Y. Xu, M. Shen, Y. Chen, Y. Lou, R. Luo, J. Chen, Y. Zhang, J. Li, W. Wang, Optimization of the polysaccharide hydrolysate from *Auricularia auricula* with antioxidant activity by response surface methodology, Int. J. Biol. Macromol. 113 (2018) 543–549, https://doi.org/10.1016/j.ijbiomac.2018.02.059.
[22] L. Liang, G. Liu, F. Zhang, Q. Li, R.J. Linhardt, Digestibility of squash polysaccharide under simulated salivary, gastric and intestinal conditions and its impact on short-chain fatty acid production in type-2 diabetic rats, Carbohydr. Polym. 235 (2020) 115904, https://doi.org/10.1016/j.carbpol.2020.115904.
[23] D. Qu, S. Wang, H. Zhao, H. Liu, D. Zhu, L. Jiang, Structure and interfacial adsorption behavior of soy hull polysaccharide at the oil/water interface as influenced by pH, Food Hydrocoll. 116 (2021) 106638, https://doi.org/10.1016/j.foodhyd.2021.106638.
[24] Z. Wu, J. Wu, R. Zhang, S. Yuan, Q. Lu, Y. Yu, Colloid properties of hydrophobic modified alginate: surface tension, ζ-potential, viscosity and emulsification, Carbohydr. Polym. 181 (2018) 56–62, https://doi.org/10.1016/j.carbpol.2017.10.052.
[25] A. Mavani, D. Ray, V.K. Aswal, J. Bhattacharyya, Application of drug aggregation to solubilize antimicrobial compound and enhancing its bioavailability, Appl. Biochem. Biotechnol. 195 (2023) 3206–3216, https://doi.org/10.1007/s12010-022-04298-5.
[26] Y. Feng, S.R. Kilker, Y. Lee, Chapter seven - surface charge (zeta-potential) of nanoencapsulated food ingredients, in: S.M. Jafari (Ed.), Charact, Nanoencapsulated Food Ingred., Academic Press, 2020, pp. 213–241, https://doi.org/10.1016/B978-0-12-815667-4.00007-9.
[27] S. Gea-Botella, B. Moreno-Chamba, L. De La Casa, J. Salazar-Bermeo, N. Martí, M. C. Martínez-Madrid, M. Valero, D. Saura, Carotenoids from persimmon juice processing, Food Res. Int. 141 (2021) 109882, https://doi.org/10.1016/j.foodres.2020.109882.
[28] W. Brand-Williams, M.E. Cuvelier, C. Berset, Use of a free radical method to evaluate antioxidant activity, LWT - Food Sci. Technol. 28 (1995) 25–30, https://doi.org/10.1016/S0023-6438(95)80008-5.
[29] T. Belwal, P. Dhyani, I.D. Bhatt, R.S. Rawal, V. Pande, Optimization extraction conditions for improving phenolic content and antioxidant activity in *Berberis asiatica* fruits using response surface methodology (RSM), Food Chem. 207 (2016) 115–124, https://doi.org/10.1016/j.foodchem.2016.03.081.
[30] L.N. Hiliţanu, L. Mititelu-Tarţău, E.G. Popa, B.R. Bucă, I.L. Gurzu, P.A. Fotache, A.-M. Pelin, D.A. Pricop, L.L. Pavel, Chitosan soft matter vesicles loaded with acetaminophen as promising systems for modified drug release, Molecules 29 (2024) 57, https://doi.org/10.3390/molecules29010057.
[31] M. Minekus, M. Alminger, P. Alvito, S. Ballance, T. Bohn, C. Bourlieu, F. Carrière, R. Boutrou, M. Corredig, D. Dupont, C. Dufour, L. Egger, M. Golding, S. Karakaya, B. Kirkhus, S. Le Feunteun, U. Lesmes, A. Macierzanka, A. Mackie, S. Marze, D. J. McClements, O. Ménard, I. Recio, C.N. Santos, R.P. Singh, G.E. Vegarud, M.S. J. Wickham, W. Weitschies, A. Brodkorb, A standarised static *in vitro* digestion method suitable for food – an international consensus, Food Funct. 5 (2014) 1113–1124, https://doi.org/10.1039/C3FO60702J.
[32] B. Moreno-Chamba, J. Salazar-Bermeo, M. Narváez-Asensio, P. Navarro-Simarro, D. Saura, M. Neacsu, N. Martí, M. Valero, M.C. Martínez-Madrid, Polyphenolic extracts from *Diospyros kaki* and *Vitis vinifera* by-products stimulate cytoprotective effects in bacteria-cell host interactions by mediation of transcription factor Nrf2, Phytomedicine 134 (2024) 156020, https://doi.org/10.1016/j.phymed.2024.156020.
[33] J. Salazar-Bermeo, B. Moreno-Chamba, M.C. Martínez-Madrid, D. Saura, M. Valero, N. Martí, Potential of persimmon dietary fiber obtained from byproducts as antioxidant, prebiotic and modulating agent of the intestinal epithelial barrier function, Antioxidants 10 (2021) 1668, https://doi.org/10.3390/antiox10111668.
[34] J.R. Jørgensen, F. Yu, R. Venkatasubramanian, L.H. Nielsen, H.M. Nielsen, A. Boisen, T. Rades, A. Müllertz, *In vitro*, *ex vivo* and *in vivo* evaluation of microcontainers for oral delivery of insulin, Pharmaceutics 12 (2020), https://doi.org/10.3390/pharmaceutics12010048.
[35] S.F. Ng, J. Rouse, D. Sanderson, G. Eccleston, A comparative study of transmembrane diffusion and permeation of ibuprofen across synthetic membranes using Franz diffusion cells, Pharmaceutics 2 (2010) 209–223, https://doi.org/10.3390/pharmaceutics2020209.
[36] A.M. Sadeghi, M.R. Avadi, S. Ejtemaimehr, S. Abashzadeh, A. Partoazar, F. Dorkoosh, M. Faghihi, M. Rafiee-Tehrani, H.E. Junginger, Development of a gas empowered drug delivery system for peptide delivery in the small intestine, J. Control. Release 134 (2009) 11–17, https://doi.org/10.1016/j.jconrel.2008.10.012.
[37] A.B. Sánchez, A.C. Calpena, M. Mallandrich, B. Clares, Validation of an *ex vivo* permeation method for the intestinal permeability of different BCS drugs and its correlation with caco-2 *in vitro* experiments, Pharmaceutics 11 (2019) 638, https://doi.org/10.3390/pharmaceutics11120638.
[38] P. Costa, J.M.S. Lobo, Modeling and comparison of dissolution profiles, Eur. J. Pharm. Sci. 13 (2001) 123–133, https://doi.org/10.1016/s0928-0987(01)00095-1.
[39] Z. Li, Y. Wang, Y. Pei, W. Xiong, C. Zhang, W. Xu, S. Liu, B. Li, Curcumin encapsulated in the complex of lysozyme/carboxymethylcellulose and implications for the antioxidant activity of curcumin, Food Res. Int. 75 (2015) 98–105, https://doi.org/10.1016/j.foodres.2015.05.058.
[40] L. Saulnier, M.-J. Crépeau, M. Lahaye, J.-F. Thibault, M.T. Garcia-Conesa, P. A. Kroon, G. Williamson, Isolation and structural determination of two 5,5′-diferuloyl oligosaccharides indicate that maize heteroxylans are covalently cross-linked by oxidatively coupled ferulates, Carbohydr. Res. 320 (1999) 82–92, https://doi.org/10.1016/S0008-6215(99)00152-4.
[41] S.N.S. Othman, A.N. Mustapa, K.H. Ku-Hamid, Extraction of polyphenols from *Clinacanthus nutans Lindau* (*C. Nutans*) by vacuum solvent-free microwave extraction (V-SFME), Chem. Eng. Commun. 208 (2020) 727–740, https://doi.org/10.1080/00986445.2020.1727452.
[42] Y. Wang, D. Li, L.-J. Wang, S.-J. Li, B. Adhikari, Effects of drying methods on the functional properties of flaxseed gum powders, Carbohydr. Polym. 81 (2010) 128–133, https://doi.org/10.1016/j.carbpol.2010.02.005.
[43] F.A.N. Fernandes, T.V. Fonteles, S. Rodrigues, E.S. de Brito, B.K. Tiwari, Ultrasound-assisted extraction of anthocyanins and phenolics from jabuticaba (*Myrciaria cauliflora*) peel: kinetics and mathematical modeling, J. Food Sci. Technol. 57 (2020) 2321–2328, https://doi.org/10.1007/s13197-020-04270-3.
[44] C. Chen, L.J. You, A.M. Abbasi, X. Fu, R.H. Liu, Optimization for ultrasound extraction of polysaccharides from mulberry fruits with antioxidant and hyperglycemic activity in vitro, Carbohydr. Polym. 130 (2015) 122–132, https://doi.org/10.1016/j.carbpol.2015.05.003.
[45] X. Fan, H. Chang, Y. Lin, X. Zhao, A. Zhang, S. Li, Z. Feng, X. Chen, Effects of ultrasound-assisted enzyme hydrolysis on the microstructure and physicochemical properties of okara fibers, Ultrason. Sonochem. 69 (2020) 105247, https://doi.org/10.1016/j.ultsonch.2020.105247.
[46] C. Zhu, X. Liu, Optimization of extraction process of crude polysaccharides from pomegranate peel by response surface methodology, Carbohydr. Polym. 92 (2013) 1197–1202, https://doi.org/10.1016/j.carbpol.2012.10.073.
[47] K. Peng, Y. Li, Y. Sun, W. Xu, H. Wang, R. Zhang, Y. Yi, Lotus root polysaccharide-phenol complexes: interaction, structure, antioxidant, and anti-inflammatory activities, Foods 12 (2023) 577, https://doi.org/10.3390/foods12030577.
[48] N. Muñoz-Almagro, M. Vendrell-Calatayud, P. Méndez-Albiñana, R. Moreno, M. P. Cano, M. Villamiel, Extraction optimization and structural characterization of pectin from persimmon fruit (*Diospyros kaki* Thunb. Var. Rojo brillante),

Carbohydr. Polym. 272 (2021) 118411, https://doi.org/10.1016/j.carbpol.2021.118411.
[49] T.K. Patle, K. Shrivas, R. Kurrey, S. Upadhyay, R. Jangde, R. Chauhan, Phytochemical screening and determination of phenolics and flavonoids in *Dillenia pentagyna* using UV–vis and FTIR spectroscopy, Spectrochim. Acta A Mol. Biomol. Spectrosc. 242 (2020) 118717, https://doi.org/10.1016/j.saa.2020.118717.
[50] S. Liu, M. Jia, J. Chen, H. Wan, R. Dong, S. Nie, M. Xie, Q. Yu, Removal of bound polyphenols and its effect on antioxidant and prebiotics properties of carrot dietary fiber, Food Hydrocoll. 93 (2019) 284–292, https://doi.org/10.1016/j.foodhyd.2019.02.047.
[51] X. Liu, C.M.G.C. Renard, S. Bureau, C. Le Bourvellec, Revisiting the contribution of ATR-FTIR spectroscopy to characterize plant cell wall polysaccharides, Carbohydr. Polym. 262 (2021) 117935, https://doi.org/10.1016/j.carbpol.2021.117935.
[52] D. Ying, M.M. Hlaing, J. Lerisson, K. Pitts, L. Cheng, L. Sanguansri, M.A. Augustin, Physical properties and FTIR analysis of rice-oat flour and maize-oat flour based extruded food products containing olive pomace, Food Res. Int. 100 (2017) 665–673, https://doi.org/10.1016/j.foodres.2017.07.062.
[53] M. Liu, J. Wang, K. Yang, Y. Qi, J. Zhang, M. Fan, X. Wei, Optimization of ultrasonic-assisted extraction of antioxidant tannin from young astringent persimmon (*Diospyros kaki* L.) using response surface methodology, J. Food Process. Preserv. 42 (2018) e13657, https://doi.org/10.1111/jfpp.13657.
[54] T. Wahyono, D.A. Astuti, I.K.G. Wiryawan, I. Sugoro, A. Jayanegara, Fourier transform mid-infrared (FTIR) spectroscopy to identify tannin compounds in the panicle of sorghum mutant lines, IOP Conf. Ser. Mater. Sci. Eng. 546 (2019) 042045, https://doi.org/10.1088/1757-899X/546/4/042045.
[55] H. Ye, L. Luo, J. Wang, K. Jiang, T. Yue, H. Yang, Highly galloylated and A-type prodelphinidins and procyanidins in persimmon (*Diospyros kaki* L.) peel, Food Chem. 378 (2022) 131972, https://doi.org/10.1016/j.foodchem.2021.131972.
[56] Y. Zhang, X. Li, L. Gong, Z. Xing, Z. Lou, W. Shan, Y. Xiong, Persimmon tannin/graphene oxide composites: fabrication and superior adsorption of germanium ions in aqueous solution, J. Taiwan Inst. Chem. Eng. 104 (2019) 310–317, https://doi.org/10.1016/j.jtice.2019.08.024.
[57] Z. Xue, Y. Chen, Y. Jia, Y. Wang, Y. Lu, H. Chen, M. Zhang, Structure, thermal and rheological properties of different soluble dietary fiber fractions from mushroom *Lentinula edodes* (Berk.) Pegler residues, Food Hydrocoll. 95 (2019) 10–18, https://doi.org/10.1016/j.foodhyd.2019.04.015.
[58] I.P.S. Fernando, K.K.A. Sanjeewa, W. Samarakoon, W.W. Lee, H.-S. Kim, E.-A. Kim, U.K.D.S.S. Gunasekara, D.T.U. Abeytunga, C.M. Nanayakkara, E.D. de Silva, H.-S. Lee, Y.-J. Jeon, FTIR characterization and antioxidant activity of water soluble crude polysaccharides of Sri Lankan marine algae, Algae (2017), https://doi.org/10.4490/algae.2017.32.12.1.
[59] A.P. Terzyk, The influence of activated carbon surface chemical composition on the adsorption of acetaminophen (paracetamol) *in vitro*: part II. TG, FTIR, and XPS analysis of carbons and the temperature dependence of adsorption kinetics at the neutral pH, colloids surf, Physicochem. Eng. Asp. 177 (2001) 23–45, https://doi.org/10.1016/S0927-7757(00)00594-X.
[60] F. Zapata, A. López-Fernández, F. Ortega-Ojeda, G. Quintanilla, C. García-Ruiz, G. Montalvo, Introducing ATR-FTIR spectroscopy through analysis of acetaminophen drugs: practical lessons for interdisciplinary and progressive learning for undergraduate students, J. Chem. Educ. 98 (2021) 2675–2686, https://doi.org/10.1021/acs.jchemed.0c01231.
[61] M.K. Trivedi, S. Patil, H. Shettigar, K. Bairwa, S. Jana, Effect of biofield treatment on spectral properties of paracetamol and piroxicam, Chem. Sci. J. 6 (2015). https://hal.science/hal-01390464. (Accessed 3 June 2024).
[62] M. Daescu, N. Toulbe, M. Baibarac, A. Mogos, A. Lőrinczi, C. Logofatu, Photoluminescence as a complementary tool for UV-vis spectroscopy to highlight the photodegradation of drugs: a case study on melatonin, Molecules 25 (2020) 3820, https://doi.org/10.3390/molecules25173820.
[63] V.V. Alange, R.P. Birajdar, R.V. Kulkarni, Novel spray dried pH-sensitive polyacrylamide-grafted-carboxymethylcellulose sodium copolymer microspheres for colon targeted delivery of an anti-cancer drug, J. Biomater. Sci. - Polym. Ed. 28 (2017) 139–161, https://doi.org/10.1080/09205063.2016.1257083.
[64] I. Paños, N. Acosta, A. Heras, New drug delivery systems based on chitosan, Curr. Drug Discov. Technol. 5 (2008) 333–341, https://doi.org/10.2174/157016308786733528.
[65] P. Sriamornsak, J. Nunthanid, Calcium pectinate gel beads for controlled release drug delivery: II. Effect of formulation and processing variables on drug release, J. Microencapsul. 16 (1999) 303–313, https://doi.org/10.1080/026520499289031.
[66] C. Tonelli, I.I.C. Chio, D.A. Tuveson, Transcriptional regulation by Nrf2, Antioxid. Redox Signal. 29 (2018) 1727–1745, https://doi.org/10.1089/ars.2017.7342.
[67] R.W. Korsmeyer, R. Gurny, E. Doelker, P. Buri, N.A. Peppas, Mechanisms of solute release from porous hydrophilic polymers, Int. J. Pharm. 15 (1983) 25–35, https://doi.org/10.1016/0378-5173(83)90064-9.
[68] T.G. Barclay, C.M. Day, N. Petrovsky, S. Garg, Review of polysaccharide particle-based functional drug delivery, Carbohydr. Polym. 221 (2019) 94–112, https://doi.org/10.1016/j.carbpol.2019.05.067.
[69] A.M. Senna, K.M. Novack, V.R. Botaro, Synthesis and characterization of hydrogels from cellulose acetate by esterification crosslinking with EDTA dianhydride, Carbohydr. Polym. 114 (2014) 260–268, https://doi.org/10.1016/j.carbpol.2014.08.017.